



Phase-Locking and Bifurcations of the Sinusoidally-Driven Double Scroll Circuit *

MURILO S. BAPTISTA** and IBERÊ L. CALDAS

Institute of Physics, University of São Paulo, P.O. Box 66318, 05315-970 São Paulo, S.P., Brazil

(Received: 3 February 1997; accepted: 22 April 1998)

Abstract. The dynamic alterations of an electronic circuit in a chaotic regime, described by the Double Scroll attractor, subjected to sinusoidal perturbation are numerically investigated. Parameter diagrams of the circuit phase-locking oscillations in terms of the driving amplitude and frequency are computed. These diagrams have highly interleaved and complex structures, part of them Cantor-like fractals. However, a Cantor-like fractal structure is also observed. In addition, the power spectrum analysis is used to find and characterize three ways of phase-locking the Double Scroll circuit, and to determine how this process depends on the driving parameters. Furthermore, the dynamics of bifurcation phenomena, as chaotic attractor entrainment, Arnold's tongues, coexistence of attractors, and hysteresis are identified in the parameter space.

Keywords: Phase-locking, bifurcations, chaos, electronic circuits.

1. Introduction

Periodic-oscillating non-linear systems have important applications in any situation whenever predictability of complex dynamical systems is required. Besides, in many situations controlling chaotic systems by periodic forcing is useful as in the applications reported in [1–5]. Thus, determining the convenient driving parameters (usually amplitudes and frequencies) is relevant to improve the desired control or oscillation phase-locking in the considered systems. Furthermore, investigating the dependence of this effect, or other bifurcation phenomena commonly observed in such driven systems, on the required control driving parameters, is also convenient.

Electronic non-linear circuits are particularly useful to investigate these non-linear phenomena [6], as the mentioned oscillation phase-locking. In fact, these systems are experimentally easy to build, usually with very low noise levels, and their characteristic dynamics are well modeled by differential equations. Examples of experiments with a non-linear circuit perturbed by periodic forces can be seen in [7–9].

The best known non-linear electronic circuit is the Matsumoto's circuit [6] (also known as Chua's circuit). This is a simple non-linear circuit with a piecewise-linear resistor.

Several bifurcation phenomena and phase-locking properties are observed in experiments with the original Matsumoto's circuit or with slightly modified versions of this circuit [10, 11]. In particular, we mention here some of the reported features that are numerically investigated in this work. Adding one inductor and one voltage source to this circuit, it is possible to induce period-doubling bifurcations, period-adding and the Farey sequence, quasi-periodic

* Contributed by Professor D. T. Mook.

** Presently at the Institute for Plasma Research, University of Maryland, College Park, MD 20742, U.S.A.

and chaotic behavior, coexistence of multiple attractors and hysteresis [12, 13]. The same is observed if the circuit is driven by a current source, in addition with the frequency entrainment of chaos also reported in this case [14]. For this last kind of driving force, the appearance of Arnold's tongues and period-adding law in the driving parameter space is numerically observed [10].

In this paper, we consider the Matsumoto's electronic circuit in a chaotic regime described by the Double Scroll attractor, a very known attractor in the literature [6]. Therefore, in this case, this circuit is called Double Scroll circuit [16].

We investigated numerically phase-locking and bifurcation phenomena when the Double Scroll circuit was driven by a sinusoidal perturbation. The considered driving was different from those used in other works. Namely, the voltage source was applied to the linear resistor in series with the inductor. With this perturbation, we observed, both numerically and experimentally [17], all phenomena previously mentioned. However, in this work, we addressed more general questions concerning the representation of these phenomena in the driving control parameter space. Thus, we identified regions in this space with points representing the same kind of attractor behavior (periodic, quasi-periodic, or chaotic), or attractors with the same period.

Generally, the analysis of these structures in the parameter diagrams, can reveal if the application of a chosen periodic perturbation to a given system is a good method to obtain chaos suppression. One question is to determine any possible relation between the driving amplitude and frequency applied to this system and the resulting phase-locked frequency.

Particularly, for small frequencies there is the phenomenon of frequency entrainment of chaotic motion [14, 17]. However, for further smaller frequencies or almost constant perturbations, we observed another new phenomenon: the chaotic attractor cyclically visiting chaotic and periodic regions connected by a period-doubling road to chaos. In fact, this kind of trajectory reproduced the road to create the Double Scroll attractor by varying one of the control parameters [17].

Besides the previously mentioned phenomena, these parameter diagrams show also the period attractor preservation for large ranges of driving frequency and amplitude, as it can be experimentally reproduced [17].

In Section 2 we present the driven Double Scroll circuit. In Section 3 we present the algorithm used to compute the driving-parameter space diagrams. We use power spectrum analysis to show, in Section 4, that there are three different ways of phase-locking the considered oscillations. In Section 5 we analyze, for low frequencies, the periodic entrainment of chaos, the Arnold's tongues and their period-adding law in the driving-parameter space, and the coexistence of different attractors. For some of these phenomena, we show also evidences of fractal structures in the parameter space. We present the conclusions in Section 6.

2. Driven Double Scroll Circuit

The Double Scroll circuit is shown in Figure 1 with its three energetic components: two capacitors, C_1 and C_2 , and one inductor, L . It has also two resistors, R and r , and the non-linear resistor, R_{NL} , whose characteristic curve can be seen in Figure 2.

The R_{NL} characteristic curve is represented by

$$i_{NR}(V_{c1}) = m_0 V_{c1} + 0.5(m_1 - m_0)|V_{c1} + B_p| + 0.5(m_0 - m_1)|V_{c1} - B_p|, \quad (1)$$

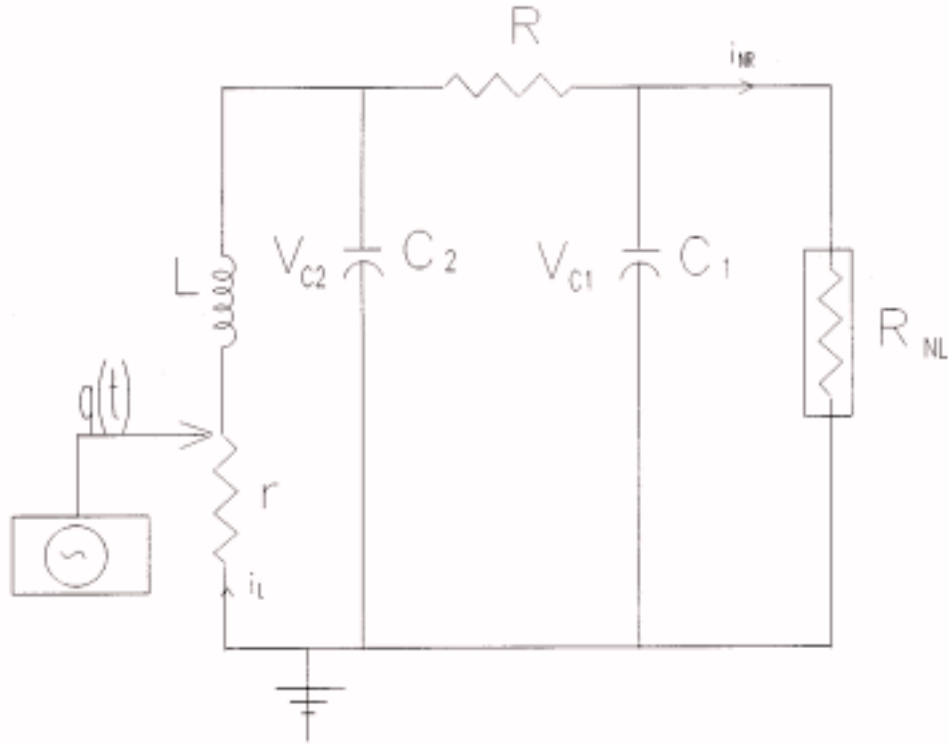


Figure 1. The Double Scroll circuit. Although, in this work, we consider only numerical results, the electronic value components used for the realization of a real experiment are: $C_1 = 0.0052 \mu\text{F}$, $C_2 = 0.056 \mu\text{F}$, $R = 1470 \Omega$, $L = 9.2 \text{ mH}$, and $r = 10 \Omega$.

where m_0 , m_1 , and B_p are indicated in Figure 2. V_{C1} is the voltage across the non-linear resistor.

The driving force applied across the resistor r (Figure 1) is represented by

$$q(t) = V \sin(2\pi ft), \quad (2)$$

where V is the amplitude and f is the frequency.

We can simulate the circuit of Figure 1 by applying Kirchoff's laws. So, the resulting state equations are

$$\begin{aligned} C_1 \frac{dV_{C1}}{dt} &= \frac{1}{R} (V_{C2} - V_{C1}) - i_{NR}(V_{C1}) \\ C_2 \frac{dV_{C2}}{dt} &= \frac{1}{R} (V_{C1} - V_{C2}) + i_L \\ L \frac{di_L}{dt} &= -V_{C2} - q(t), \end{aligned} \quad (3)$$

where V_{C1} and V_{C2} are the voltage across the capacitors C_1 and C_2 , respectively, and i_L is the electric current across the inductor L . To avoid numerical problems we do not use the actual component values in Equations (3), but a rescaled set of parameters given in terms of

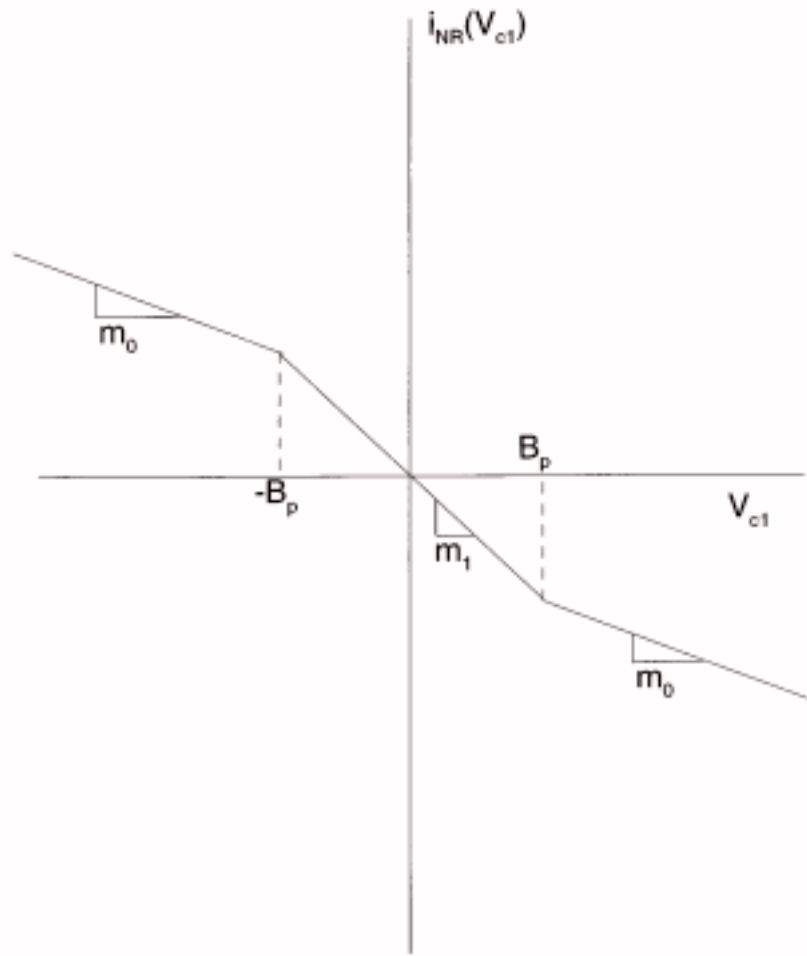


Figure 2. The characteristic curve of the non-linear resistor R_{NL} , where $B_p = 1.0$, $m_0 = -0.5$, and $m_1 = -0.8$.

the actual values. Thus, in this work, the parameters used in Equations (3) for the numerical simulation of the circuit in Figure 1 are

$$\frac{1}{C_1} = 10.0, \quad \frac{1}{C_2} = 1.0, \quad \frac{1}{L} = 6.0, \quad \frac{1}{R} = 0.6 \quad (4)$$

and the normalized initial conditions are

$$V_{c1}(0) = 0.15264, \quad V_{c2} = -0.02281, \quad i_L(0) = 0.38127. \quad (5)$$

For the parameter simulation values given by Equation (4), and for a vanishing perturbing amplitude $V = 0$, the circuit behaves chaotically. As the circuit is dissipative its dynamic variables (V_{C1} , V_{C2} , and i_L) evolve on a chaotic attractor named Double Scroll that can be seen in Figure 3.

All results shown in this paper are due to numerical simulations. However, we also built the circuit of Figure 1 and observed the bifurcation phenomena here discussed. For further details about this experiment we refer to [18].

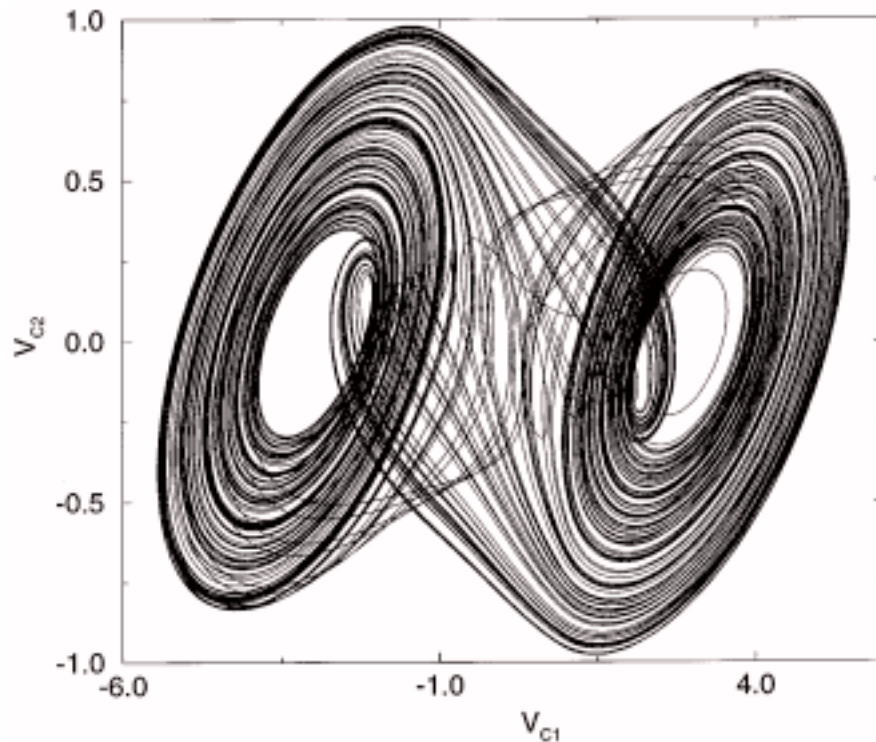


Figure 3. The chaotic Double Scroll attractor for $V = 0$ and other parameters given by Equations (4) and (5).

3. Parameter Space Diagrams

We chose to investigate the behavior of the driven Double Scroll system in the Poincaré section on the plane $V_{C1} = -1.5$. Thus, instead of dealing with the trajectories, we analyzed the mapping determined by their intersections on the Poincaré section. We obtained a good convergence when the transient length was $n = 100$, where n is the number of times the trajectory crosses the Poincaré section.

For obtaining the parameter space diagrams two methods were considered.

The most known tool for constructing a parameter space diagram is the Lyapunov spectrum formed by the three Lyapunov exponents λ_n . For the considered system, the nature of the attractor can be characterized by the values of these three Lyapunov exponents: $(\lambda_1, \lambda_2, \lambda_3)$. Thus, a chaotic oscillation, for which $\lambda_1 > 0$, $\lambda_2 = 0$, $\lambda_3 < 0$, is represented as $(+, 0, -)$. Moreover, $(0, 0, -)$ stands for a quasi-periodic movement on a torus T^2 , $(0, -, -)$ represents a limit cycle, and $(-, -, -)$ represents a fixed point.

We obtained the Lyapunov exponents by applying the Eckmann–Ruelle algorithm [19, 20] with a transient $n = 100$, and a time step $dt = 0.005$ during a integration time $t = 3882$ which corresponds to $n \approx 700$. The Gram–Schmidt orthonormalization is applied each $GS = 10$ steps.

Due to the non-exact computation of these exponents, we consider an exponent null if its value is within the interval $[-\varepsilon, \varepsilon]$, where $\varepsilon = 0.02$, if we consider the previous parameters of the algorithm. However, such parameters force us to wait a large CPU time to obtain each Lyapunov spectrum with the desired accuracy.

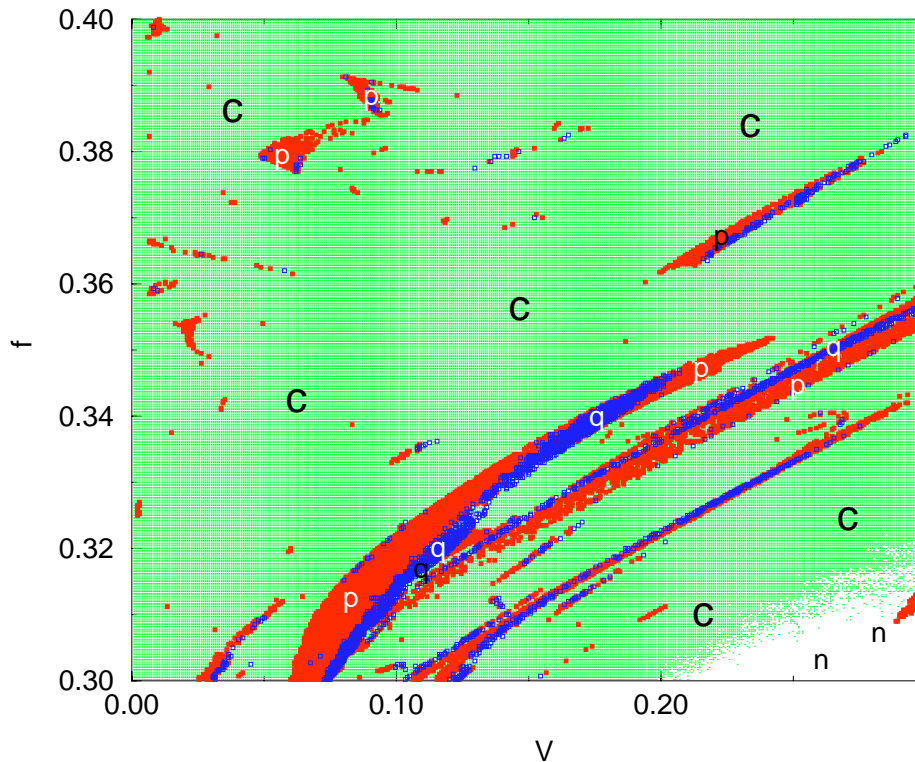


Figure 4. Parameter space diagram ($f \times V$) obtained from the Lyapunov spectra, indicating the behavior of the driven Double Scroll system through different level of gray. Letter c indicates chaotic oscillations, letter p indicates periodic oscillations, letter q indicates quasi-periodic oscillations, and letter n indicates trajectories that go to infinity. We used a 400×400 grid of points.

So, we determined that similar results, but not so faithful, can be obtained if we consider $dt = 0.04$, $t = 1040$ which correspond to $n \approx 260$, and $GS = 15$. The tolerance considered is still $\varepsilon = 0.02$. With these considerations in mind we obtained the parameter space diagram shown in Figure 4, where 400 values of the frequency and amplitude were considered.

In this figure we can see for which value of f or V we have chaos (black region indicated by c), limit cycles (clear gray region indicated by p), or tori T^2 (dark gray region indicated by q). We also found unbounded trajectories (the white region indicated by the letter n) due to exterior crises [21]. In this figure, the minimum value of f is close to the value of the characteristic frequency $f_c \approx 0.29$ for the unperturbed system ($V = 0$), corresponding to $f_c \approx 5.40$ kHz.

The use of the Eckmann–Ruelle algorithm has basically three main problems: the large amount of CPU time required, the incapability of detecting weak chaos (the toroidal chaos that is due to the breakdown of a two-frequency torus through the Curry–Yorke scenario [20] for which the largest Lyapunov exponent is too small, and the impossibility of determining the period of the periodic orbits.

There is an additional problem with the Eckmann–Ruelle algorithm. It works very well for autonomous systems; however, when we have a non-autonomous case (as when the sinusoidal perturbation is introduced into the Double Scroll system), the choice of t , n , GS , and dt for a specific f and V may not be convenient for another set of these parameters. Hence, for

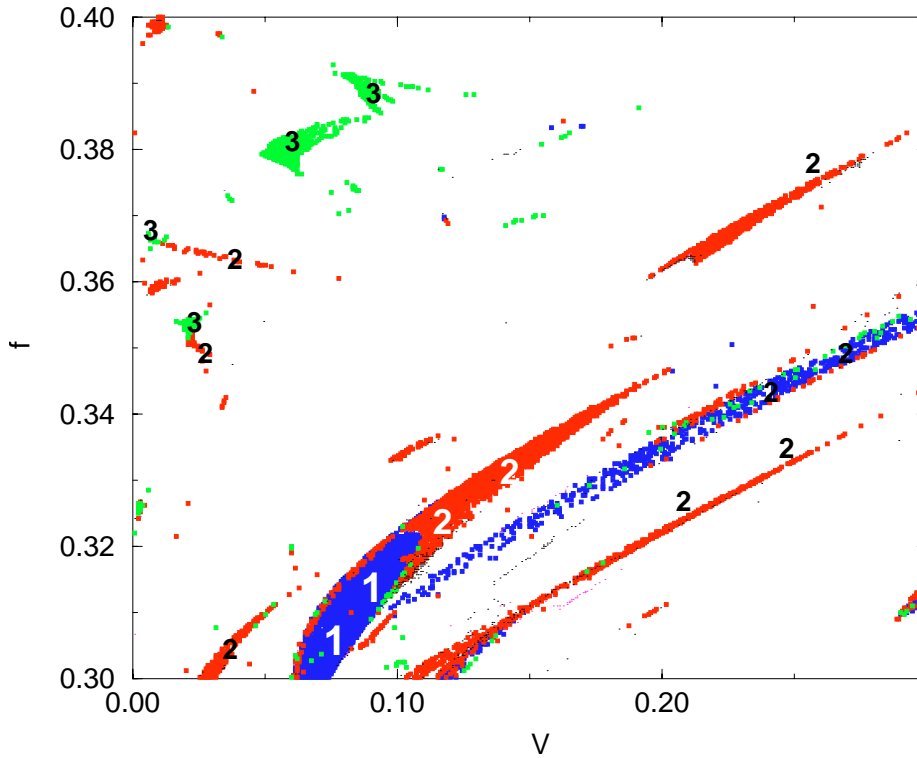


Figure 5. Parameter space diagram indicating the period, indicated by numbers, of orbits of the driven Double Scroll system. A 400×400 grid of points is considered in this figure.

computing a parameter space for which a large range of f and V must be considered, the use of another algorithm may be more convenient.

So, we realized that in our case an algorithm that identifies only the periodic regions would be appropriate for our understanding of the driven Double Scroll system. This can be confirmed by the fact that small quasi-periodic regions of the parameter space (for the driven Double Scroll system) always surround periodic regions (therefore, regions that are neither periodic nor quasi-periodic are surely chaotic, disregarding the non-finite trajectories). Also, in this work, we have not identified orbits with periods higher than $p_{\max} = 16$, because they are not significant.

In order to determine whether an orbit is p -periodic on a Poincaré surface we proceeded as follows. After the transient (100 crossings in the Poincaré section) we keep the next $n = p_{\max} + k$ points (X_n , with $i = 1, \dots, p_{\max} + k$, where X represents the coordinates V_{C2} and i_L , on the Poincaré section $V_{C1} = -1.5$) to verify whether the coordinate values repeat themselves p times. Thus, we compute

$$\text{accum} = \sum_{n=1}^k |X_n - X_{n+p}|, \quad (6)$$

for $p = (1, 2, 3, \dots, 16)$.

We considered that we have a period- p orbit if, for the minimum p , and for $k = 5$, $\text{accum} < 0.02$. In Figure 5 we show a diagram where the period- p regions, obtained by using

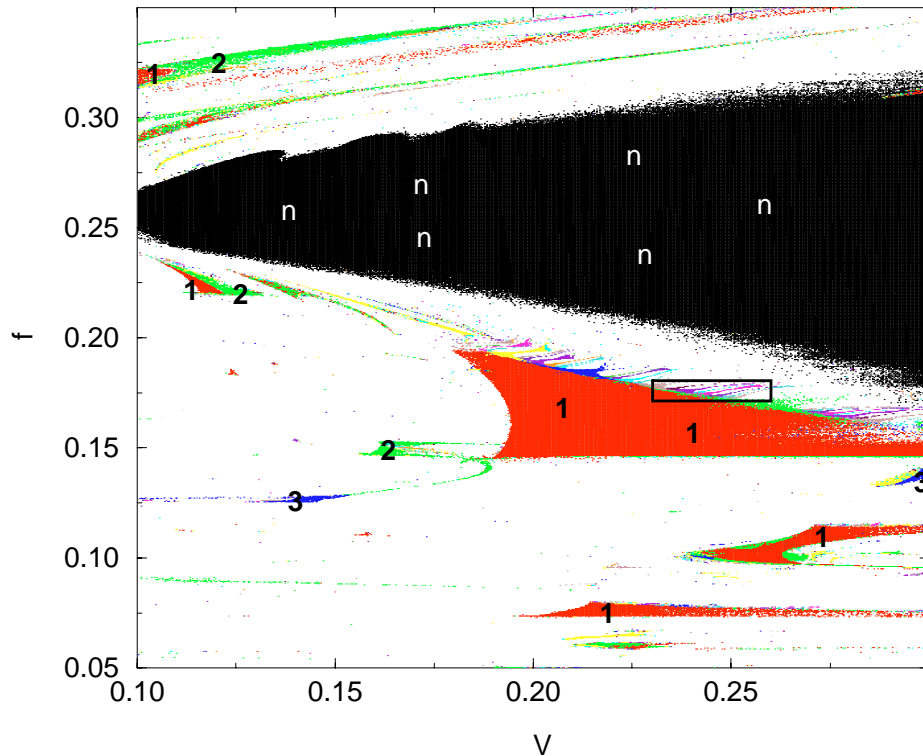


Figure 6. Isoperiodic diagram showing the period of the orbits of the driven Double Scroll system. The regions marked by the letter n represent values of frequency and amplitude for which no bounded attractor was obtained. A 800×600 grid of points is considered in this figure.

the algorithm (6), are indicated by the numbers and with different gray scales. This figure has the same range of f and V as Figure 4.

Besides the suitable CPU time spent for computing Figure 5 (about four times smaller than the previous Eckmann–Ruelle algorithm using Gram–Schmidt), we can now precisely identify the period- p regions in the parameter space.

Figure 6 shows a diagram considering another range of V and f that will be investigated in this paper. In this figure, we see a large region (the largest black region, indicated with the letter n) corresponding to non-finite trajectories. We also see periodic regions (with the period indicated by numbers) and specially a large period-one island (indicated by the number 1) that is a region where we find periodic movement for a large varying amplitude and frequency. In this case, for a large varying frequency or amplitude only small changes are induced in the shape of the period-one orbits.

4. Phase-Locking

We aimed to study chaos suppression caused by driving perturbations in the Double Scroll circuit. We identified three ways through which periodic movement is induced in this system: two from chaotic and one from quasi-periodic oscillations. These ways are identified according to the position of the merging frequency peak in the power spectra when a periodic oscillation

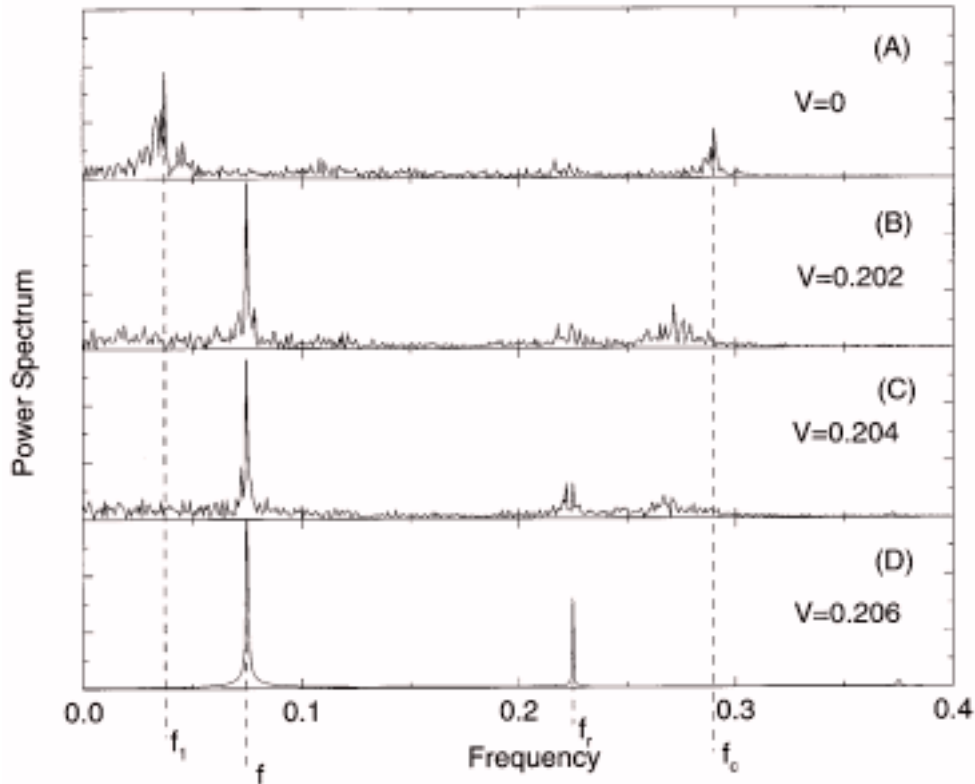


Figure 7. Power spectra of the time evolution of the variable V_{C1} , for frequency $f = 0.075$ and different amplitudes V , to show the phasing-locking at the driving frequency f . (A) shows the characteristic frequencies, f_1 , and f_c , of the unperturbed circuit. Rising V (B, C, D) the peaks f_c and f_1 disappear and the frequencies f and f_r show up.

shows up. The power spectra showed hereon were computed using the FFT algorithm for the time evolution of the variable V_{C1} . We considered 32768 points.

Figure 7A shows the spectrum of the unperturbed system. We see two main peaks, one corresponding to the characteristic frequency $f_c \approx 0.29$ and the other, indicated by f_1 , corresponding to the frequency with which the trajectory jumps between the two rolls presented in the Double Scroll attractor. For $f = 0.075$ and $V = 0.202$, in Figure 7B, the peak at f_1 is destroyed and a peak corresponding to the driving frequency appears. In addition, the peak f_c moves to the left. The amplitude of this moving peak decreased as we increased V to 0.204, in Figure 7C, and a small peak became evident at f_r . Finally, when we set $V = 0.206$ the system is periodic and the spectrum has only two peaks, with the harmonic frequencies f and f_r representing the driving frequency and the response frequency, respectively. In this case the orbit is a limit cycle.

In Figure 8 we see a series of spectra showing for a varying amplitude how the periodic movement appeared. In this case both peaks, with f_c and f_1 (Figure 8A), had their amplitudes decreased (Figures 8B and 8C), being completely destroyed when $V = 0.20$ (Figure 8D). In this last figure there is only one peak, corresponding to the driving frequency f .

The values of $V = 0.20$ and $f = 0.17$ correspond to the large period-one island showed in Figure 6. For any set of parameters, f and V , of this island, the obtained attractor has only

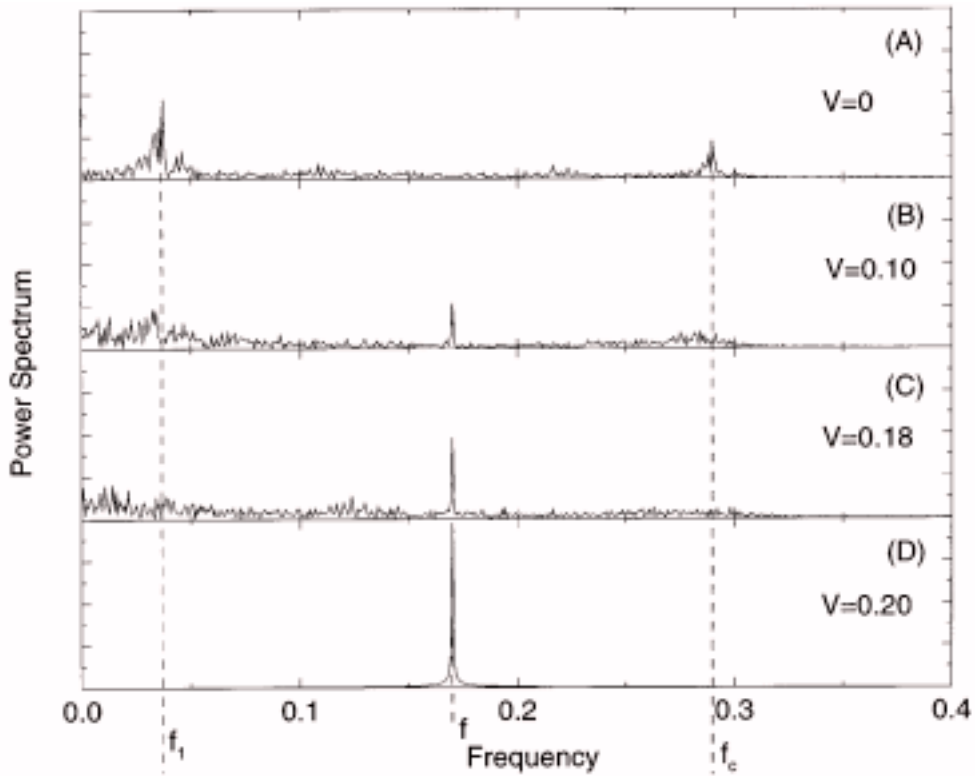


Figure 8. Power spectra of the time evolution of the variable V_{C1} , for frequency $f = 0.17$ and different amplitudes V , to show the phasing-locking at the driving frequency f . (A) shows the characteristic frequencies, f_1 , and f_c , of the unperturbed circuit. Rising V (B, C, D) the peaks f_c and f_1 disappear and the frequency f shows up.

the driving frequency f . This result shows that for such driving perturbations the circuit has responses characteristics of linear circuits.

Until now we showed periodic regimes for which the frequency components f_c and f_1 are destroyed. However, we observed that, if we choose a frequency f harmonic to f_c or f_1 , these last frequencies may be preserved.

So, in Figure 9 we see that, when we introduced the perturbation with $f = 0.650$ and $V = 0.08$ (Figure 9B), the perturbed spectra is still similar to the one shown in Figure 9A. The peak corresponding to $f = 0.650$, inside the small box, had a very small amplitude, indicating that the driving had a small effect on the Double Scroll system. Increasing the driving frequency to $f = 0.652$ (and fixing $V = 0.08$) we got periodic movement. Naturally, in these cases the peaks f_r and f_1 had a frequency harmonic to the frequency f .

Thus, if perturbing the system with a frequency harmonic to f_c we get periodic movement, the resulting trajectory has frequencies very close to harmonics of the frequencies f_c and f_1 . This fact led us to think that the resulting trajectory preserves some characteristics of the unperturbed attractor, as it can be seen in Figure 10 where we plot an unstable periodic orbit of the non-perturbed Double Scroll system (the thin line) and the perturbed orbit with $f = 0.652$ and $V = 0.08$.

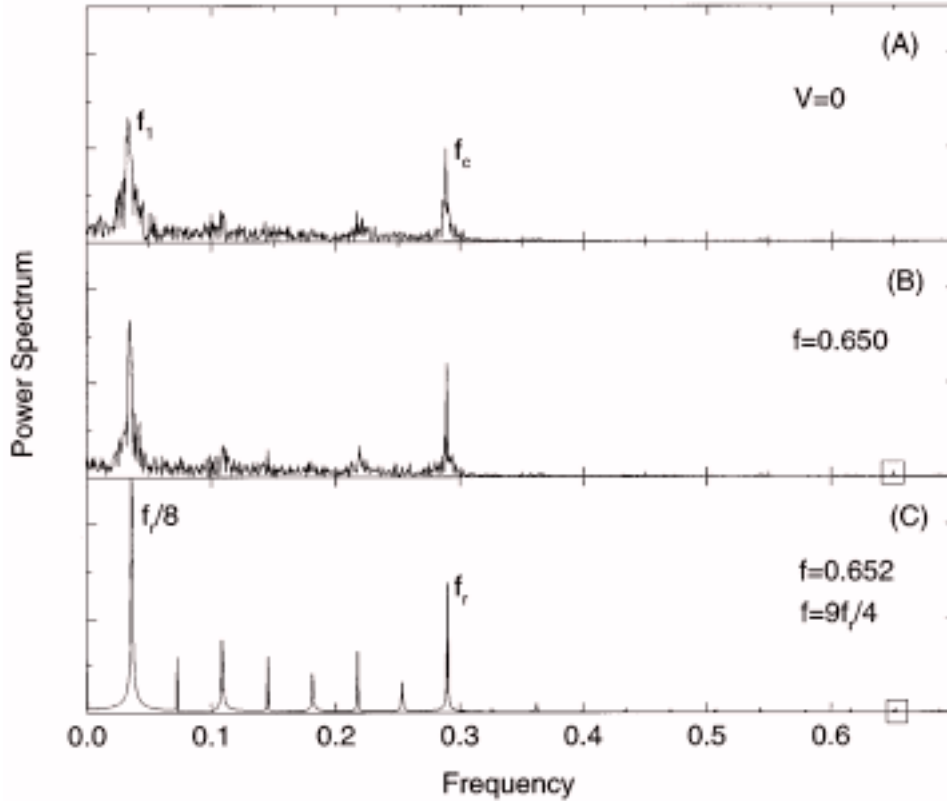


Figure 9. Power spectra of the time evolution of the variable V_{C1} , for amplitude $V = 0.08$ and different frequencies f , to show the phasing-locking at the driving frequency f . (A) shows the characteristic frequencies, f_1 , and f_c , of the unperturbed circuit. Rising f (B, C) the peaks f_c and f_1 are preserved, the peak corresponding to f has a very small amplitude indicated on the box, and f_r with its harmonics show up.

In this system, there is another way through which periodic movement can appear from a quasi-periodic movement. In this case we have two incommensurable frequencies that phase-locks as showed in the next section.

5. Bifurcation Phenomena

5.1. PERIODIC ENTRAINMENT OF CHAOTIC ATTRACTORS

For perturbations with small driving frequencies, we did not find any periodic regime. However, there is one interesting phenomenon where a chaotic trajectory tracks a periodic oscillation, named periodic entrainment of the chaotic attractor.

As a matter of fact, the system (3) has three equilibrium points whose positions and equilibrium stability are changing in time according to the value of the driving perturbation $q(t)$. Thus, this driven system for a null perturbation has the equilibrium points: P^1 , a stable 1D saddle and an unstable 2D saddle, P^2 , a 1D unstable saddle and a 2D stable focus, and P^3 , the same as P^1 , each corresponding to one of the three domains of the function (1).

The position of these points in respect to $q(t)$ is given by

$$P^1 = (-\alpha - \beta, q(t), g\alpha - m_0\beta), \quad P^2 = (-\gamma, -q(t), -m_1\gamma),$$

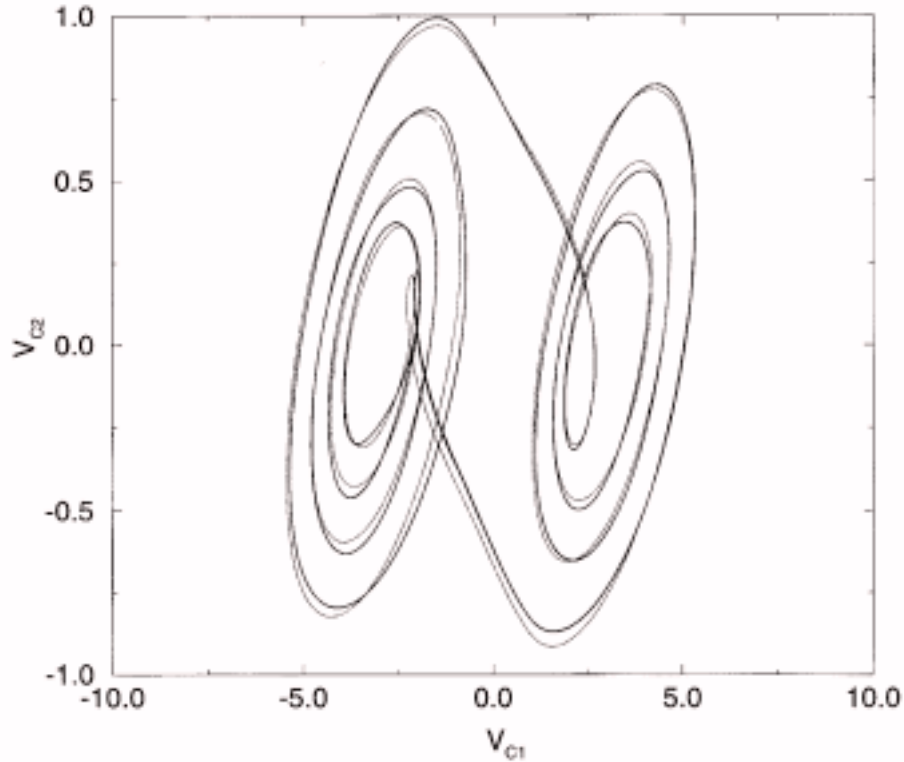


Figure 10. The unstable periodic orbit of the non-perturbed Double Scroll system (the thin line) and the orbit obtained for driving parameters $f = 0.652$ and $V = 0.08$, showing that stabilization of chaotic oscillation using the driving sinusoidal perturbation can preserve the original features of the non-perturbed system.

$$P^3 = (\alpha - \beta, -V, -g\alpha - m_0\beta), \quad (7)$$

where

$$\alpha = \frac{B_p(m_0 - m_1)}{(g + m_0)}, \quad \beta = \frac{B_p(m_0 - m_1)}{g + m_0}, \quad \text{and} \quad \gamma = \frac{gq(t)}{g + m_1}.$$

To see this periodic entrainment, in Figure 11 we plot the time evolution of the variable V_{C1} and the corresponding values of the first coordinate of the equilibrium points X^1 , X^2 , and X^3 . We note that the trajectory evolves with the driving period around the equilibrium points. In addition, the attractor seems to change in successive small time intervals (smaller than the period of the perturbing term $q(t)$), as it can be seen in Figure 12.

Figure 12 shows the trajectory during eight successive time intervals ($\delta t = 32$). The first V_{C1} plotted value in these figures can be identified, in Figure 11, by the letters inside boxes.

We see that Figure 12A represents a trajectory that resembles a limit cycle. This happens because the equilibrium point P^3 changes its position with the equilibrium point P^2 (see Figure 11). In fact, there is such a limit cycle for a constant perturbation $q = \mp 0.4$ correspondent to an average value of q in the intervals containing the points A and H of Figure 11.

In Figure 12 the trajectory resembles that of the Double Scroll attractor, with the trajectory oscillating around the two different points P^1 and P^3 . In fact, the time evolution from Figures 12A to 12D shows a time period-doubling routes to chaos. The time-reversed period-

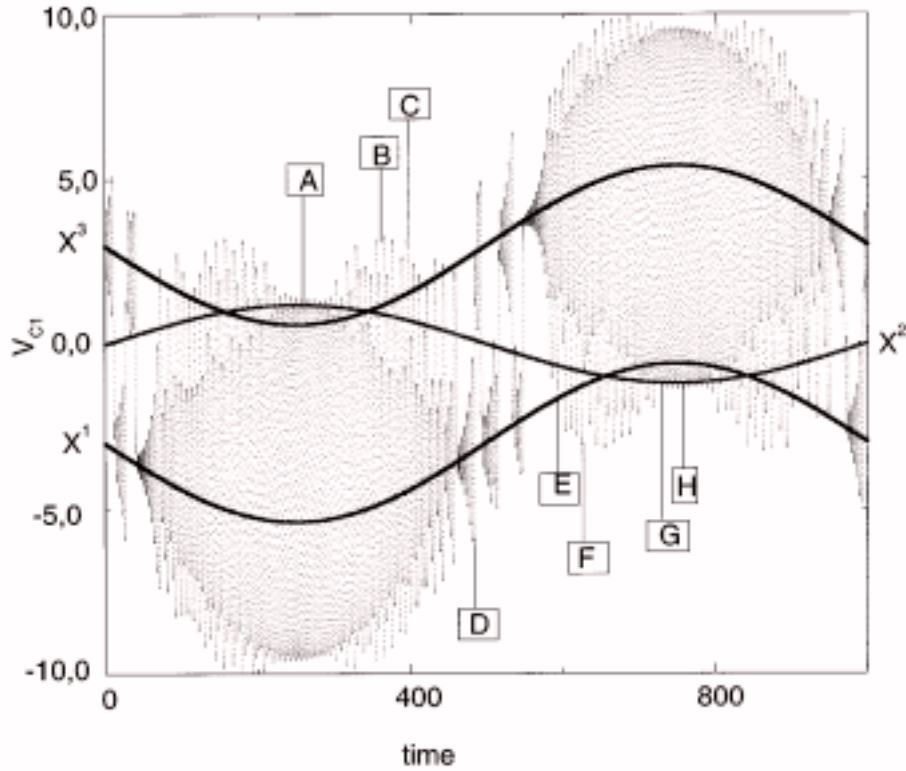


Figure 11. Time evolution of the variable V_{C1} of the system (3) with $f = 0.001$ and $V = 0.4$. The first coordinates of the equilibrium points (X^1 , X^2 , and X^3) whose position change in time due to the perturbation are also plotted. We see that the trajectory evolves along these points.

doubling bifurcations can be seen in Figures 12D–12H. In other words, the analyzed chaotic trajectory visits different embedded attractors.

If we consider a constant amplitude we observed that we can suppress chaotic motion of the driven Double Scroll circuit by changing the position of the equilibrium points.

5.2. ARNOLD'S TONGUE AND PERIOD ADDING LAW

When the driving force is turned on, that means $V \neq 0$, a new frequency is introduced in the characteristic oscillations of the Double Scroll System. This new frequency is responsible for the appearance of quasi-periodic and periodic movements on a two-frequency torus (T^2).

In the parameter diagrams, beside periodic regions, there exist also quasi-periodic regions. Between the regions that represent a quasi-periodic trajectory, there exist regions that represents the phase-locked trajectories that evolves on the previous existing torus T^2 . These period- p regions may form what is known as Arnold's tongues [10].

These Arnold's tongues appear following a rule called period-adding law [10]. The geometrical interpretation of this law is represented by the known Farey tree. To introduce the adding law, let us first define the winding number W ,

$$W = \frac{q}{p}, \tag{8}$$

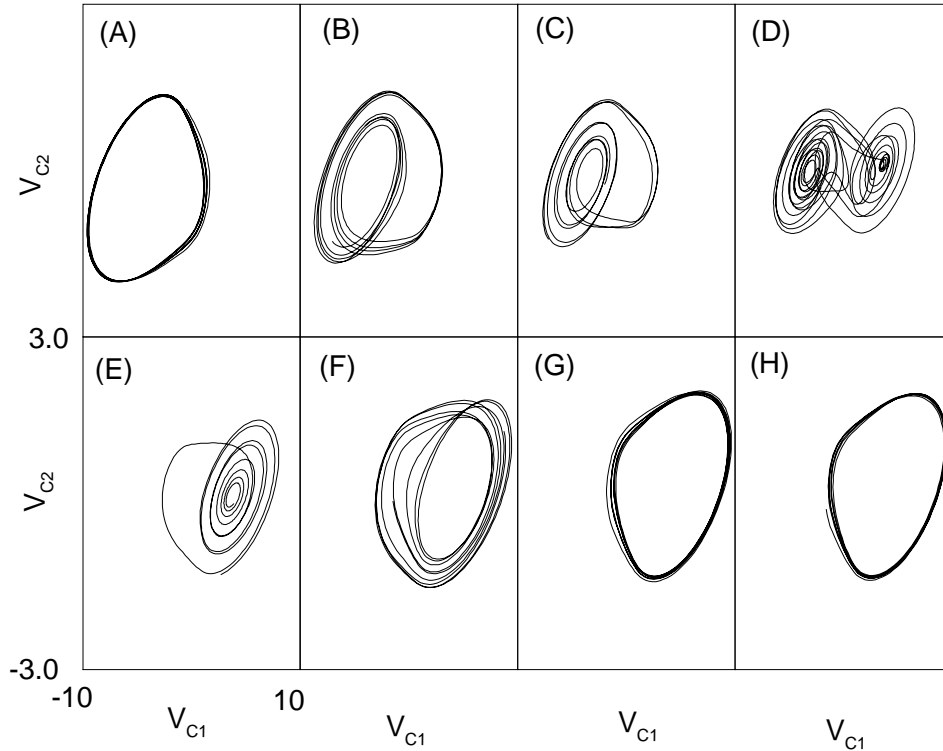


Figure 12. Time evolution of the bi-dimensional ($V_{C1} \times V_{C2}$) projection of the three-dimensional trajectory of the driven Double Scroll system with the same parameters of Figure 11. Figures A–H are obtained for intervals with $\delta t = 32$ and initial condition indicated in Figure 11 by the letters A–H.

where q is the number of the trajectory rotations along the torus to return back to the same point, taking p complete cycles. It means that p is the period of the orbit.

Following the notation [10], between two Arnold's tongues of winding number q/p and Q/P , respectively, there exist other Arnold's tongues with winding number given by

$$\begin{aligned} \frac{q}{p} &\rightarrow \frac{q+Q}{p+P} \rightarrow \frac{q+2Q}{p+2P} \rightarrow \dots \\ \frac{q+nQ}{p+nP} &\rightarrow \dots \text{chaos} \rightarrow \frac{Q}{P}. \end{aligned} \tag{9}$$

The following sequence is also valid

$$\begin{aligned} \frac{q}{p} &\leftarrow \text{chaos} \leftarrow \dots \frac{nq+Q}{np+P} \leftarrow \dots \\ \frac{2q+Q}{2p+P} &\leftarrow \frac{q+Q}{p+P} \leftarrow \frac{Q}{P}. \end{aligned} \tag{10}$$

Thus, between two prime (level I) winding numbers, a series of Arnold's tongues (level II) show up. Otherwise, between any two tongues in level II, another series of tongues may appear with their winding number classified as level III. Each level correspond to a branch in the Farey tree that can theoretically have infinity branches.

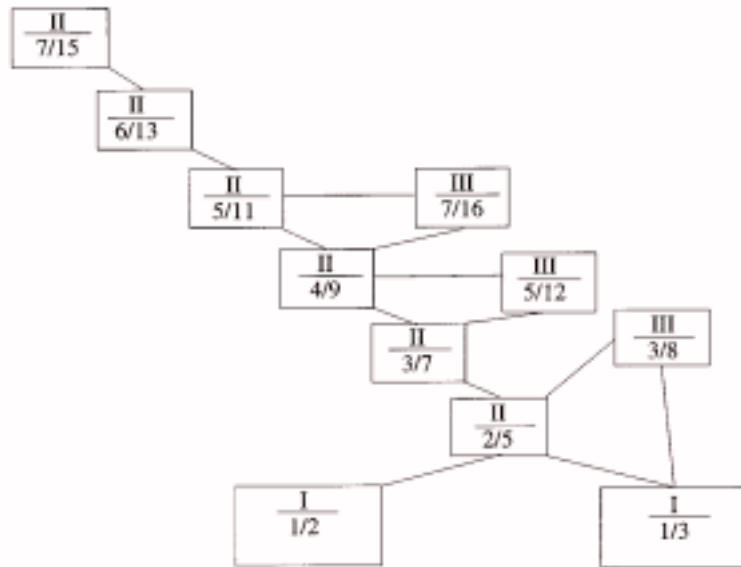


Figure 13. Schematic representation of the Farey tree constructed from the rational numbers $1/2$ and $1/3$.

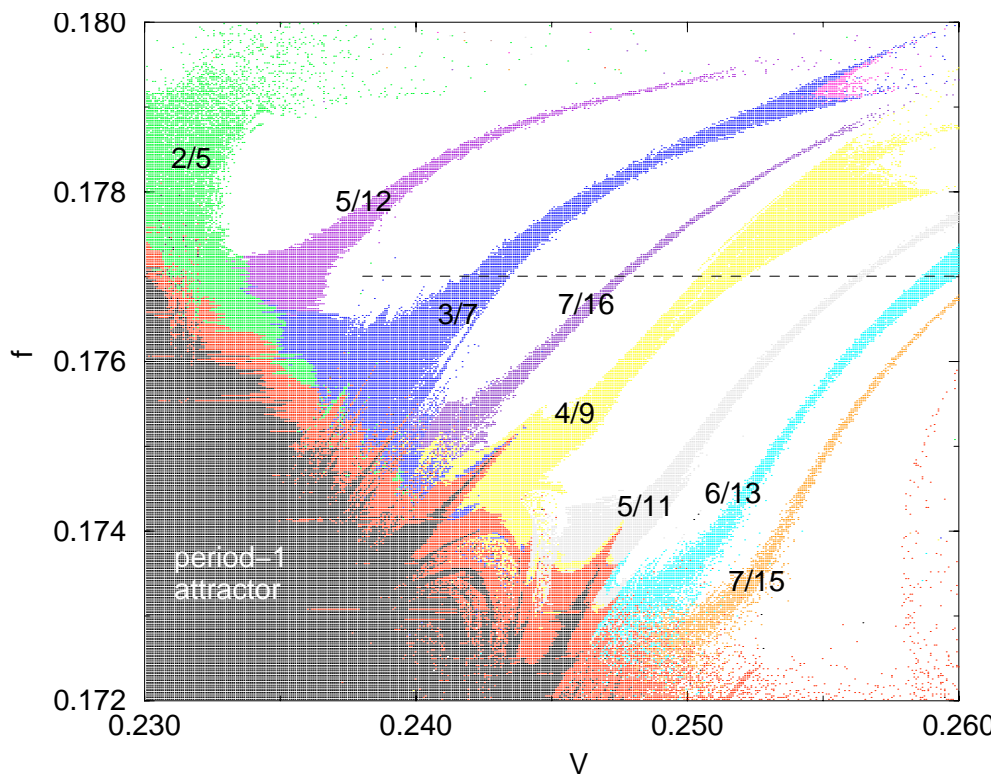


Figure 14. Magnification of Figure 6 showing the Arnold's tongues with their winding numbers indicated in the figure. These winding numbers follow the period-adding law.

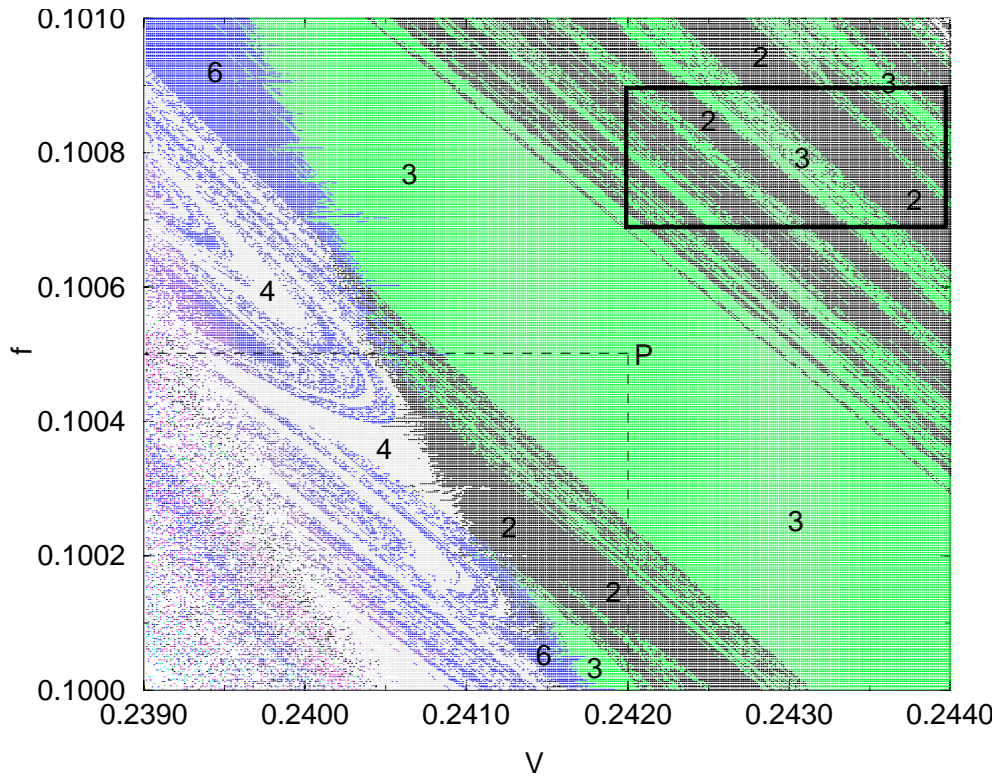


Figure 15. Magnification of Figure 6 showing the complex structure of the parameter space diagram.

In Figure 13 we represent a Farey tree where the Roman numerals indicate the branch level and the Arabian numbers, the winding number. Note that the period-adding law is verified to occur at a given level since the period- p Arnold's tongue have their periods following an arithmetic progression.

The Farey tree showed in Figure 13 is one of the many verified to occur in the studied system as it can be seen in Figure 14, a magnification of the box in Figure 6. In Figure 14, we see part of the period-one island and, when period-one trajectory suffers a Hopf bifurcation leading to the creation of a torus T^2 , the Arnold's tongues corresponding to phase-locked trajectories are observed.

5.3. COEXISTENCE OF ATTRACTORS AND HYSTERESIS

It is known that the Arnold's tongues can overlap for certain ranges of f and V [22] and thus the existence of different attractors is possible. Consequently, in the parameter space diagram this coexistence of attractors creates complex and interleaved periodic regions with fractal boundaries.

Another magnification of Figure 6 is shown in Figure 15. We see, by comparing the different levels of gray, that for small changes in f and V the system can present different period- p attractors. Successive amplifications of the box in Figure 15 show that the boundary between the period-three and period-two regions, and also the boundary between the period-four and period-six regions have a Cantor-like fractal structure. However, there are also regions of two

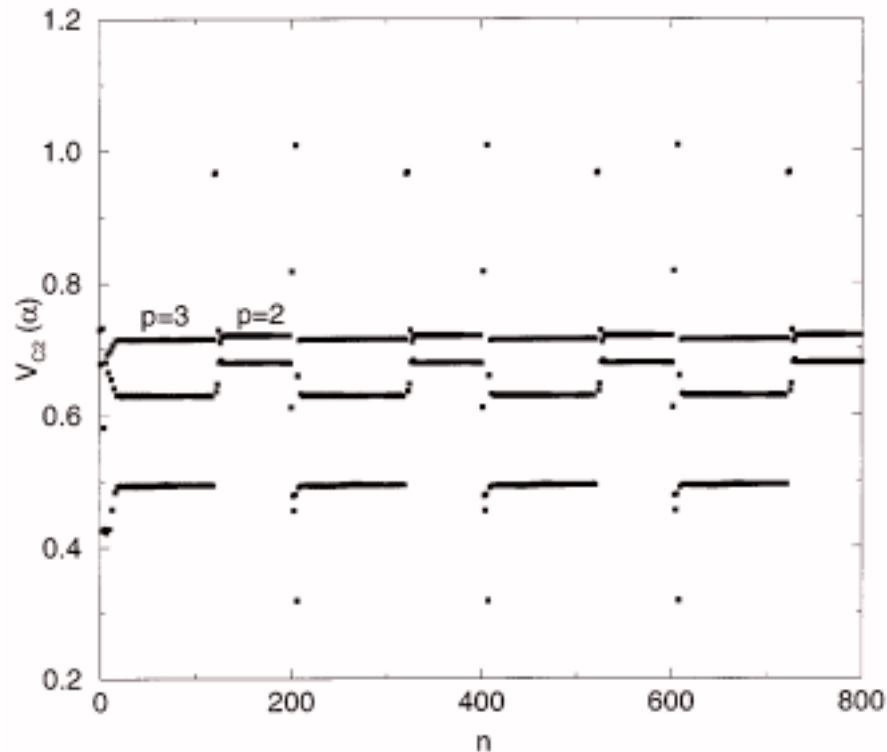


Figure 16. Time evolution of the variable V_{C2} when the trajectory crosses the Poincaré section $V_{C1} = -1.5$, for $f = 0.1005$ and $V = 0.2420$. This values correspond to the region indicated by the point P in Figure 15.

different attractors whose boundary has a non-fractal structure as we can see in Figure 6, for the boundary between periodic and chaotic regions.

Another case where we find a non-fractal boundary between regions that represents two different attractors is when one of the attractors raised from a period-doubling bifurcation of the other.

Even though the diagram of Figure 15 at the point P indicates a period-three attractor, a period-two attractor coexists as we can see in Figure 16, where it is plotted the time evolution of the variable V_{C2} when the trajectory crosses the Poincaré section $V_{C1} = -1.5$, for $f = 0.1005$ and $V = 0.2420$ (corresponding to the point P). In this figure, to change from one attractor to the other, we restarted the integration of Equation (2) with initial conditions as the last variables of the prior trajectory. The fast transients can be seen in Figure 16.

We have also observed that all periodic regions presents an attractor robust to small changes in f and V . For example, the point P in Figure 15 represents a period-three attractor, and with small changes in f and V one never obtain the other coexisting period-two attractor. Therefore, even in the presence of more than one attractor, the microscopic structure of a periodic region (far away from the boundary with another attractor) is not fractal.

The coexistence of attractors leads to the phenomenon of hysteresis due to jumps between coexisting attractors. To show that, in Figure 17, for $f = 0.075$ and a varying amplitude, we see that the system can present, for the rising amplitude (Figures 17A–17F), a different sequence of attractors obtained for the decreasing amplitude (Figures 17F–17G). Thus, for $V = 0.30$ two different attractors can be obtained (Figures 17D and 17G).

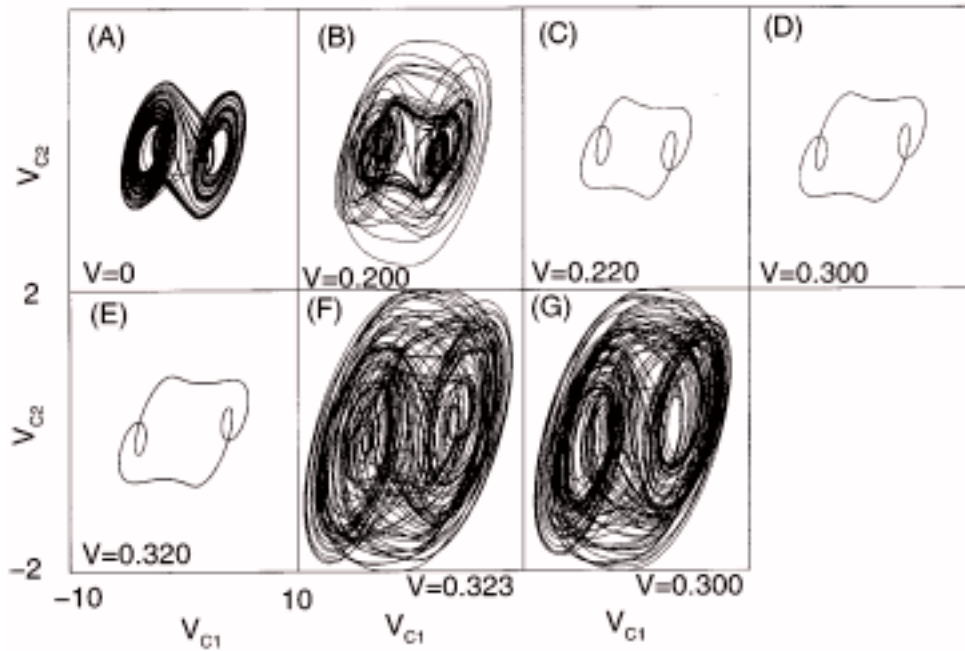


Figure 17. Sequence of attractors showing the phenomenon of hysteresis. For a fixed frequency $f = 0.075$ and a varying amplitude indicated in the figure we show that the attractor can jump to the others existing attractors.

6. Conclusions

For the purpose of having a better understanding of the phase-locking in the Double Scroll circuit [6, 16] driven by a sinusoidal perturbation [10, 12–14] we computed original and precise parameter space diagrams for ample ranges of the driving parameters.

We computed the Lyapunov spectra to distinguish if the driven circuit trajectory was chaotic, periodic or quasi-periodic. However, this kind of diagram required a large amount of computation time and an algorithm parameter dependence on the driving parameters (f and V).

We also computed these parameter diagrams considering another algorithm to identify the orbit periods. For this kind of diagram, the required CPU time was about ten times shorter than that necessary to compute the diagrams based on the Lyapunov spectrum.

With such a diagram we have complete knowledge of the phase-locked regions. With fine resolutions, many bifurcation phenomena presented in this circuit [12–14] as period-doubling, hysteresis, coexistence of attractors, phase-locking, and Arnold's tongue [10] were identified [17].

These diagrams may have regions of different attractors for which either a fractal or a non-fractal boundary may be found. Basically, a non-fractal boundary is found when the two closed regions have attractors with period p and $2p$, respectively. That means that the period- $2p$ attractor appears from its neighbor period- p suffers a period-doubling bifurcation. Another situation where there is no fractal boundary is found when you have a periodic region beside a chaotic region. This is a typical case when a tangent bifurcation occurs.

However, we also see regions of different attractors in these diagrams for which their boundary has a Cantor-like fractal structure. This is due to the coexistence of different attractors.

If the perturbing frequency, f , is smaller than the characteristic frequency, f_c , chaotic oscillations were easily suppressed, since the large-sized periodic islands presented in Figure 6 appear only for $f < f_c$. In fact, for $f > f_c$, the only structures in the parameter space are line-shaped lines, indicating that there are specific values of f to obtain periodic motion. Generally, the driving frequencies required for phase-locking are close to harmonics of the characteristic frequency f_c .

We determined three ways through which periodic motion appears for a suitable variation on the driving parameters: two when the driven circuit has a chaotic trajectory and one when it has a quasi-periodic trajectory. These three ways were newly classified according to the way the frequency peaks (in the power spectra of such chaotic or quasi-periodic trajectories) change their position with the driving parameters variation.

These three ways must be considered as the possible scenarios for the phase-locking. Therefore, if one needs to suppress chaotic motion by applying a sinusoidal perturbation, the identification of one of these three scenarios, by inspecting the power spectra of a given sinusoidally-driven system, permits to suitably adjust the driving parameter to obtain periodic motion.

The first scenario occurs when the driven circuit presents a trajectory with many frequencies harmonic to the perturbing frequency f and different from the original characteristic frequency f_c . Thus, the region of the biggest period-one island in Figure 6 has an attractor whose all frequencies f_n are given by $f_n = (2n + 1)f$; however, the only significant frequency is $f_0 = f$ because its peak amplitude is remarkably bigger than the others. That means, in this case, the circuit response to the driving is typically linear. This and other islands that appear for $f < f_c$ show the preservation of the periodic attractor for a large variation of the driving frequency and amplitude. We observed this kind of phase-locking (both, experimentally and numerically) when $f \lesssim f_c$. A special case is when $f \approx f_c$. In this case, a periodic oscillation (a period-one limit cycle resembling a circle) is obtained with the lowest amplitude V . Obviously, a periodical driven system is expected to modulate with the external frequency if its value is close to the non-perturbed characteristic frequency.

The other phase-locking scenario is when the resulting frequencies are close or harmonics of f_c and the peak of the driving frequency almost does not appear in the spectra. In this case, the driven circuit possess a trajectory that shadows an unstable periodic orbit of the non-perturbed attractor. In other words, the perturbing frequency f is close to an harmonic of f_c . Numerically, we have observed that this case usually happens when f is bigger than f_c .

The last scenario occurs when periodic motion emerges from a quasi-periodic one. In this case, the quasi-periodic trajectory evolves along a two-frequency torus, and, for a driving parameter variation, the two-orbit components phase-lock and then periodic motion shows up. The phase-locked two-frequency torus is responsible for the appearance of the Arnold's tongues [10, 12] in the parameter space diagrams around the periodic islands. Therefore, as for other systems [22], Arnold's tongues only appear beside a periodic island.

Analyzing the phenomenon of periodic entrainment of chaotic motion [14, 23, 24] we found an attractor that presented in sequential time intervals (smaller than the perturbing period) doubling routes to chaos and a time-reversed period-doubling bifurcations. In other words, this trajectory visited different embedded attractors found in non-linear systems [25].

Finally, although we analyzed sinusoidal perturbations applied to the driven Double Scroll circuit, we obtained also similar results applying other periodical perturbations (as triangular and square waves, for example) to this circuit.

Acknowledgments

The authors thank the computational assistance of Dr. W. P. de Sá (University of São Paulo), Professor Dr. R. Viana (Federal University of Paraná) for his useful suggestions, and Ms. M. Baptista for kindly revising the manuscript. This work was partially supported by FAPESP and CNPq.

References

1. Azevedo, A. and Rezende, S. M., 'Controlling chaos in Spin-wave instabilities', *Physical Review Letters* **66**, 1991, 1342–1345.
2. Braiman, Y. and Goldhirsch, I., 'Taming chaotic with weak periodic perturbations', *Physical Review Letters* **66**, 1991, 2545–2548.
3. Lima, R. and Pettini, M., 'Suppression of chaos by resonant parametric perturbations', *Physical Review A* **41**, 1990, 726–733.
4. Fronzoni, L., Giocondo, M., and Pettini, M., 'Experimental evidence of suppression of chaos by resonant parametric perturbations', *Physical Review A* **43**, 1991, 6483–6486.
5. Weltmann, K.-D., Klinger, T., and Wilke, C., 'Experimental control of chaos in a periodically driven glow discharge', *Physical Review E* **52**, 1995, 2106–2109.
6. Matsumoto, T. and Chua, L. O., 'The double scroll', *IEEE Transactions of Circuits and Systems CAS-32*, 1985, 797–818.
7. Richetti, P., Argoul, F., and Arneodo, A., 'Type-II intermittency in a periodically driven nonlinear oscillator', *Physical Review A* **34**, 1986, 726–729.
8. Huang, J.-Y. and Kim, J.-J., 'Type-II intermittency in a coupled nonlinear oscillator: Experimental observation', *Physical Review A* **36**, 1987, 1495–1497.
9. San-Martín, J. and Antoranz, J. C., 'Type-II intermittency with a double reinjection channel: Multintermittency', *Physics Letters A* **219**, 1986, 69–73.
10. Pivka, L., Zheleznyak, A. L., and Chua, L. O., 'Arnold's tongue, Devil's staircase, and self-similarity in the driven Chua's circuit', *International Journal of Bifurcation and Chaos* **4**, 1994, 1743–1753.
11. Halle, K. S., Chua, L. O., Anishenko, V. S., and Safonova, M. A., 'Signal amplification via chaos: Experimental evidence', *International Journal of Bifurcation and Chaos* **2**, 1992, 1011–1020.
12. Murali, K. and Lakshmanan, M., 'Bifurcation and chaos of the sinusoidally-driven Chua's circuit', *International Journal of Bifurcation and Chaos* **1**, 1991, 369–384.
13. Murali, K. and Lakshmanan, M., 'Transition from quasiperiodicity to chaos and Devil's staircase structures of the driven Chua's circuit', *International Journal of Bifurcation and Chaos* **2**, 1992, 621–632.
14. Itoh, M. and Murakami, H., 'Experimental study of forced Chua's oscillator', *International Journal of Bifurcation and Chaos* **4**, 1994, 1721–1742.
15. Shil'nikov, L. P., 'Chua's circuit: Rigorous results and future problems', *International Journal of Bifurcation and Chaos* **4**, 1994, 489–519.
16. Hayes, S., Grebogi, C., and Ott, E., 'Communicating with chaos', *Physical Review Letters* **70**, 1993, 3031–3034.
17. Baptista, M. S., 'Perturbing non-linear systems, an overview for controlling chaos', Ph.D. Thesis, Universidade de São Paulo, IFUSP, 1996.
18. Baptista, M. S. and Caldas, I. L., 'Type-II intermittence in the driven double scroll circuit', submitted.
19. Eckmann, J. P. and Ruelle, D., 'Ergodic theory of chaos', *Reviews of Modern Physics* **57**, 1985, 617–656.
20. Bergé, P., *Le Chaos: Théorie et Expériences*, Eyrolles, Paris, 1988.
21. Grebogi, C. and Ott, E., 'Crisis, sudden changes in chaotic attractors, and transient chaos', *Physica D* **7**, 1983, 181–200.

22. Aronson, D. G., Chory, M. A., Hall, G. R., and McGehee, R. P., 'Bifurcations from invariant circle for two-parameter families of maps of the plane: A computer-assisted study', *Communications in Mathematical Physics* **83**, 1982, 303–354.
23. Jackson, E. A. and Hübner, A., 'Periodic entrainment of chaotic logistic map dynamics', *Physica D* **44**, 1990, 407–420.
24. Jackson, E. A. and Kodozeorgiou, A., 'Entrainment and migration controls of two-dimensional maps', *Physica D* **54**, 1992, 253–265.
25. Hunt, B. R. and Ott, E., 'Optimal periodic orbits of chaotic systems', *Physical Review Letters* **76**, 1996, 2254–2257.